

From Weakly to Strongly Magnetized Isotropic MHD Turbulence

Alexandros Alexakis

*Laboratoire de Physique Statistique de l'Ecole Normale Supérieure,
UMR CNRS 8550, 24 Rue Lhomond, 75006 Paris Cedex 05, France.*

(Dated: June 28, 2018)

High Reynolds number isotropic magneto-hydro-dynamic turbulence in the presence of large scale magnetic fields is investigated as a function of the magnetic field strength. For a variety of flow configurations the energy dissipation rate ϵ follows the Kolmogorov scaling $\epsilon \propto U_{rms}^3/\ell$ even when the large scale magnetic field energy is twenty times larger than the kinetic. Further increase of the magnetic energy showed a transition to the $\epsilon \propto U_{rms}^2 B_{rms}/\ell$ scaling implying that magnetic shear becomes more efficient at this point at cascading the energy than the velocity fluctuations. Strongly helical configurations form helicity condensates that deviate from these scalings. Weak turbulence scaling was absent from the investigation. Finally, the magnetic energy spectra showed support for the Kolmogorov spectrum $k^{-5/3}$ while kinetic energy spectra are closer to the Iroshnikov-Kraichnan spectrum $k^{-3/2}$.

One of the most fundamental questions that can be asked about an out-of-equilibrium system is the relation between the energy injection/dissipation rate ϵ , and the amplitude of the fluctuations u_ℓ . In hydrodynamic turbulence such estimates are clear and the desired relation comes from the balance between the injection rate and the flux of energy to the small scales due to nonlinear interactions. Such considerations lead to the turbulent scaling $\epsilon \propto u_\ell^3/\ell$ for $Re \propto u_\ell \ell/\nu \gg 1$. Here ν is the kinematic viscosity, u_ℓ is the amplitude of the velocity fluctuations at the forcing scale $\ell = \ell_F$. Constancy of the energy flux over all scales ℓ leads to $u_\ell \propto \epsilon^{1/3} \ell^{1/3}$ that results to the Kolmogorov (K41) prediction for the energy spectrum $E(k) = C_K \epsilon^{2/3} k^{-5/3}$ [1]. Although the proportionality coefficient C_K for the turbulent scaling is still debatable in the literature [2], the scaling is well supported by both experiments and numerical simulations [3, 4].

The situation becomes more complex when a linear wave term is introduced in the dynamical equations. Such terms introduce new timescales in the system and the validity of the previously derived relations is in question. If the amplitude of the wave frequency ω is sufficiently larger than the amplitude of the fluctuation shear u_ℓ/ℓ then the system can be treated within the framework of weak turbulence theory [5]. Then depending on the wave resonances (three-wave, four-wave etc) the energy injection rate is decreased and becomes

$$\epsilon \propto C \frac{u_\ell^3}{\ell} \left(\frac{u_\ell/\ell}{\omega} \right)^n \quad (1)$$

where $n = 0$ for strong turbulence and $n = 1$ for three-wave interactions [5]. As the strength of the wave term is increased a transition is expected from the Kolmogorov scaling for which the energy dissipation rate scales like the fluctuation amplitude to the cubic power to the weak turbulent scaling where higher powers are involved.

Magneto-Hydro-Dynamic (MHD) turbulence is an example of turbulence where eddies and (Alfven) waves co-exist [6, 7], and provides a good approximation to a variety of industrial and astrophysical flows [8, 9]. When

a flow is coupled to a uniform magnetic field B_0 fluctuations travel parallel or anti-parallel to the magnetic field lines with $\omega \propto \pm B_0/\ell_\parallel$. The indexes \perp, \parallel indicate the direction perpendicular and parallel to the magnetic field respectively. The nonlinearities allow for three wave interactions [10] and the scaling $\epsilon = Cu_\ell^4/B_0\ell$ is expected. If isotropy is assumed ($\ell_\perp \sim \ell_\parallel \sim \ell$), constant energy flux over all scales ℓ implies $u_\ell \propto (\epsilon B_0 \ell)^{1/4}$ that leads to Iroshnikov-Kraichnan (IK) energy spectrum $E(k) \propto (\epsilon B_0)^{1/2} k^{-3/2}$ [11, 12].

However the assumption of isotropy that was assumed is not valid in the presence of a strong magnetic field that suppresses the cascade in its direction [13]. For strong turbulence K41 arguments can be repeated taking into account anisotropy that leads to the energy spectrum $E(k) \propto \epsilon^{2/3} k_\perp^{-5/3}$ with the so called critical balance relation $u_\ell/\ell_\perp \sim B_0/\ell_\parallel$ [14]. An anisotropic IK energy spectrum can also be recovered $E(k) \propto \epsilon^{2/3} k_\perp^{-2/3}$ by assuming that the proportionality coefficient \tilde{C} that appears in eq. 1 decreases with scale like $C \propto \ell_\perp^{1/4}$ due to scale dependent alignment of the two fields (velocity and magnetic) that quenches the non-linearities [15]. The two proposed spectra have been investigated, in the last years by numerical simulations [16, 17] by different groups without however reaching agreement for the strong turbulence spectrum.

Weak turbulence on the other hand valid for $u_\ell/\ell_\perp \ll B_0/\ell_\parallel$ can be treated perturbatively. Detailed calculation [10] leads to the prediction for the spectrum $E(k) \propto f(k_\parallel) k_\parallel^{1/2} (\epsilon B_0)^{1/2} k_\perp^{-2}$. However weak MHD turbulence has the particularity that all three-wave resonant interactions contain one wavenumber with zero projection in the direction of the magnetic field and zero phase velocity. The set of these wave numbers themselves compose a strongly coupled nonlinear system and thus further assumptions are needed for the validity of weak turbulence. In numerical simulations weak MHD turbulence has been observed only when the resonant manifold $k_\parallel = 0$ is not forced [18–20]. When it is forced the 2D components dominate, the turbulence is strong and can also introduce

an inverse cascade as observed in 2-dimensional flows [20].

In nature uniform magnetic fields do not exist. However, magnetic fields B_L that vary over large length-scales L can be approximated as uniform provided that turbulent energy remains in much smaller scales. The validity of this approximation however is in doubt since small scale variations $\ell_\perp \ll L$ couple to parallel variations $\ell_\parallel \sim B_L \ell_\perp / u_\ell$ that can be as large as L provided that B_L is strong enough. Then the assumption of uniformity is not valid. Thus, MHD turbulence in the presence of large scale (but not uniform) fields needs to be revisited.

To study statistically isotropic MHD turbulence in the presence of large scale magnetic fields we employ high resolution direct numerical simulations of the MHD equations:

$$\partial_t \mathbf{u} + \mathbf{u} \cdot \nabla \mathbf{u} = \mathbf{b} \cdot \nabla \mathbf{b} - \nabla P + \nu \nabla^2 \mathbf{u} + \mathbf{F}_u \quad (2)$$

$$\partial_t \mathbf{b} + \mathbf{u} \cdot \nabla \mathbf{b} = \mathbf{b} \cdot \nabla \mathbf{u} + \eta \nabla^2 \mathbf{b} + \mathbf{F}_b. \quad (3)$$

in a triple periodic box of size $L = 2\pi$. Here \mathbf{u} is the velocity field and \mathbf{b} the magnetic field. Both fields satisfy $\nabla \cdot \mathbf{u} = \nabla \cdot \mathbf{b} = 0$ and $\langle \mathbf{u} \rangle = \langle \mathbf{b} \rangle = 0$, where the angular brackets stand for spatial average. ν is the viscosity and η the magnetic diffusivity. \mathbf{F}_u is an external mechanical body force, while $\mathbf{F}_b = \nabla \times \mathcal{E}$ where \mathcal{E} is an external electromotive force. \mathbf{F}_u and \mathbf{F}_b are both solenoidal functions varying randomly in time with time correlation τ . \mathbf{F}_u is acting only on wavenumbers with $|\mathbf{k}| = k_u = 2$ and is non-helical: $\langle \mathbf{F}_u \cdot \nabla \times \mathbf{F}_u \rangle = 0$. \mathbf{F}_b is acting only in the largest scale of the system $|\mathbf{k}| = k_b = 1$, and in general has non-zero helicity. All the parameters of the runs can be found in table I. For the simulations a pseudo-spectral code was used [21, 22] on grids of size 512^3 (Runs A#) and 1024^3 (Runs B#).

In a typical helical run all quantities grow initially up to a point when dissipation rates and kinetic energy reach a steady state while the magnetic energy is still increasing slowly. During this time the magnetic field is composed of a large scale helical component B_L with $|\mathbf{k}| \simeq 1$ that contains most of the magnetic energy and small scale turbulent fluctuations b_ℓ of amplitude $b_\ell \sim u$. Thus magnetic energy E_M provides a measure of the large scale field $E_M \simeq \frac{1}{2} B_L^2$, while kinetic energy E_K provides a measure of the turbulent fluctuations. The growth of B_L depends on the amplitude and the helicity of the magnetic forcing. The time evolution of the large resolution runs can be seen in figure 1. Due to the slow increase of the magnetic energy it is possible to perform short time averages (over a few turn over times) and thus obtain global averaged quantities for various values of magnetic energy from the same run. Thus the turbulent scaling of the energy dissipation rate can be tested from multiple measurements for a wide range of magnetic field strength that here it is quantified by $\mu \equiv E_M / E_K$. The isotropy of the system also allows to perform spherical averages and thus improve two point statistics compared to the case with uniform magnetic fields.

Figure 2 shows the energy dissipation rate normalized by $U_{rms}^3 k_u = (2E_K)^{3/2} k_u$ as a function of the en-

RUNS	$\mathcal{G}^{1/2}$	\mathcal{M}	\mathcal{H}	St^{-1}	Re	\mathcal{R}_λ	μ
A1	356	0.00	-	0.50	580	157	0.4
A2	1666	0.10	0.59	0.01	905	181	0.7
A3	2500	0.00	-	0.01	1331	206	0.7
A4	1666	1.00	0.00	0.01	1064	170	1.4 - 1.7
A5	353	0.50	0.15	0.50	541	106	1.5 - 2.9
A6	353	0.50	0.31	0.50	690	151	2.4 - 3.2
A7	353	0.50	1.00	0.50	734	205	2.6 - 4.5
A8	353	0.50	0.95	0.50	645	148	2.7 - 5.0
A9	353	1.00	0.15	0.50	811	141	1.8 - 7.6
A10	1666	1.00	1.00	0.01	972	154	1.8 - 9.5
A11	1666	1.00	0.59	0.01	920	138	2.0 - 14.0
A12	1666	1.00	1.00	0.01	1877	634	5.7 - 12.0
A13	1054	10.00	0.59	0.01	1081	105	6.0 - 94.0
B1	3846	0.00	-	0.01	2813	296	0.6
B2	1414	0.50	0.31	0.5	2572	311	2.6
B3'	6123	1.00	1.00	0.01	3714	386	5.0 - 18.0
B3	6123	0.40	0.50	0.01	4105	298	18.0 - 24.0

TABLE I. Table with the parameters of all runs. The numbers in the first four columns are the input parameters given by $\mathcal{G} \equiv \langle \mathbf{F}_u^2 \rangle^{1/2} / \nu^2 k_u^3$ the Grashof number, $\mathcal{M} \equiv \langle \mathbf{F}_b^2 \rangle^{1/2} / \langle \mathbf{F}_u^2 \rangle^{1/2}$ the ratio of magnetic to mechanical forcing, $\mathcal{H} \equiv \langle \mathbf{F}_b \cdot \nabla \times \mathbf{F}_b \rangle / \langle \mathbf{F}_b^2 \rangle k_b$ the relative helicity of the forcing and $St \equiv \tau_f / \tau$ the Strouhal number where $\tau_f \equiv 1 / (\langle \mathbf{F}_u^2 \rangle k_u^2)^{1/4}$. $\mathcal{M} = 0$ imply dynamo runs. The Prandtl number $\mathcal{Pr} \equiv \nu / \eta$ for all runs was set equal to 1. The last columns give the measured parameters $Re \equiv \langle \mathbf{u}^2 \rangle^{1/2} / \nu k_u$ the Reynolds number and $\mathcal{R}_\lambda \equiv \langle \mathbf{u}^2 \rangle^{1/2} / \nu \langle (\nabla \times \mathbf{u})^2 \rangle^{1/2}$ the Taylor Reynolds number. $\mathcal{R}_\lambda \equiv \langle \mathbf{u}^2 \rangle^{1/2} \lambda / \nu$ (with $\lambda^2 \equiv \langle \mathbf{u}^2 \rangle / \langle (\nabla \times \mathbf{u})^2 \rangle$) the Taylor Reynolds number. The last column gives the range of values obtained by $\mu \equiv E_M / E_K$ the ratio of magnetic to kinetic energy. The simulations named A# were carried out in a grid of size 512^3 while the simulations named B# were carried out in a grid of size 1024^3 . The third 1024^3 -grid simulation started with the parameters of B3' and run up to $t \simeq 24$ turn over times $\tau_u \equiv 1 / k_u \langle \mathbf{u}^2 \rangle^{1/2}$. afterwards it was continued with the parameters B3.

ergy ratio μ for all the examined runs. The data cover more than two decades of the parameter μ . Three different behaviors can be observed. First, over the range μ ($0.5 \leq \mu \leq 20$) the energy dissipation is independent of μ . This implies that ϵ follows the Kolmogorov scaling $\epsilon \propto u_\ell^3 / \ell$ even when the large scale magnetic energy is twenty times greater than the turbulent kinetic energy. The data include runs that vary from fully helical to non-helical, and strongly magnetically forced to dynamo runs and for $\mathcal{R}_\lambda \sim 100$ to $\mathcal{R}_\lambda \sim 300$. Thus this result seems to be very general and robust in this range.

At μ larger than 10 two new branches appear. The results of run A12 that is fully helical and strongly magnetically forced is marked by triangles in figure 2. For this run both magnetic and kinetic energy is concentrated in the large scales building helical structures with very small turbulent fluctuations. The large scale magnetic and kinetic energy both increase with time keeping their ratio μ fixed while the small scale fluctuations and the dissipation rates saturate with time. As a result the normalized

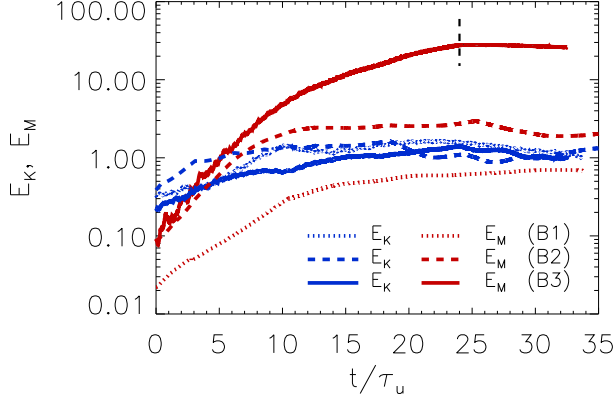


FIG. 1. Kinetic and magnetic energy evolution as a function of time for the three 1024^3 runs. The vertical dashed line indicates when the forcing parameters changed from the ones for B3' to the ones for B3.

dissipation rate $\epsilon/U_{rms}^3 k_u$ decreases with time resulting in the behavior seen in fig.2. The dynamics here are controlled by magnetic helicity condensates, and despite the large Reynolds number they do not follow a turbulent scaling.

Run A13 marked by circles in figure 2 is strongly magnetically forced in order to achieve large values of μ within the time limitations imposed by the computational costs. This run although in agreement with the turbulent scaling for $\mu \leq 20$ it transitions to the scaling $\epsilon \propto \mu^{1/2}$ as indicated by the dashed line in the figure. This scaling can be understood if we consider that the main mechanism for cascading the injected energy is not the velocity shear $S_u \propto U_{rms} k_u$ but rather the magnetic shear $S_b \propto B_{rms} k_b$ that shreds Alfvén-wavepackets as they travel along chaotic magnetic field lines. The resulting scaling is $\epsilon \propto S_b U^2 \propto U^3 k_b \mu^{1/2}$ that is observed in figure 2. Thus the large scale field rather than suppressing the turbulence cascade it enhances it.

None of the runs showed a weak turbulence scaling that would have implied according to 1 the scaling $\epsilon \propto U^4/B_L k_u \propto \mu^{-1/2}$. There are few possible interpretations for this result. First, just like the case of the uniform magnetic field, the absence of weak turbulence is can be explained by the entrapment of energy in modes that vary perpendicular to the local magnetic field so that $\ell_\perp \ll \ell_\parallel$ that makes the nonlinear coupling strong. Another possibility is the lack of uniformity of the magnetic energy density: regions exist in space with weak local magnetic field where eddies can be stretched with no resistance from magnetic tension. If the cascade in these regions dominates the scaling of turbulence becomes independent of B_L . A final possibility is that magnetic instabilities reveal themselves altering the scaling (like run A13) before the magnetic field becomes strong enough for weak turbulence to manifest itself.

The energy spectra E_m, E_k for the high resolution runs B1,B2,B3 are shown in figure 3. For the B1 dynamo run the kinetic energy spectrum shows a power-law scaling

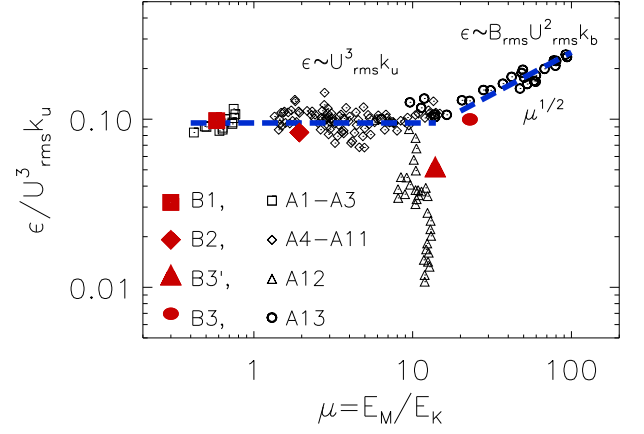


FIG. 2. Top panel: The energy dissipation rate ϵ normalized by $U_{rms}^3 k_u$ as a function of $\mu = E_M/E_K$ for all runs. $B_{rms} = \sqrt{2E_M}$ and $U_{rms} = \sqrt{2E_K}$. The dashed lines indicate the scaling $\epsilon \propto U_{rms}^3 k_u$ and $\epsilon \propto U_{rms}^2 B_{rms} k_b \propto \mu^{1/2}$.

slightly less steep than the $k^{-3/2}$ prediction. A clear change of slope is observed at $k \sim 8$ where $E_m(k)$ becomes larger than $E_k(k)$ is also observed. The magnetic energy spectrum does not show a power-law scaling. The absence of a power-law scaling might be linked to the absence of large scale magnetic structures in randomly forced dynamo runs. The B2, B3 runs despite the one order of magnitude difference in μ show similar results. The kinetic energy spectrum is well fitted by a $k^{-3/2}$ power-law while the magnetic energy spectrum is best fitted by a $k^{-5/3}$ law. The fact that different exponent is measured for the velocity and for the magnetic field indicates that probably a clear inertial range has not been reached yet even at 1024^3 grid sizes. Two reasons affect the measured spectrum exponents. First, at small wave numbers the large scale field B_L contaminates the inertial range making the spectrum look steeper. Second at large wave numbers the energy spectrum can be altered by bottle-neck effects that are far from well understood in MHD. The insets in figure 3 show the total energy flux $\Pi(q) \equiv \langle \mathbf{u}_q^< \cdot \nabla \mathbf{u} - \mathbf{b} \cdot \nabla \mathbf{b} \rangle + \mathbf{b}_q^< \cdot (\mathbf{u} \cdot \nabla \mathbf{b} - \mathbf{b} \cdot \nabla \mathbf{u}) \rangle$ [7] (solid lines) and the energy flux due to the vortex stretching term $\Pi_u(q) \equiv \langle \mathbf{u}_q^< \cdot (\mathbf{u} \cdot \nabla \mathbf{u}) \rangle$ (dashed line). $\mathbf{u}_q^<, \mathbf{b}_q^<$ are the filtered velocity field containing only wavenumbers with $|\mathbf{k}| < q$. In all three cases the vortex stretching term plays a minor role in cascading the energy.

The top panel of figure 4 shows the measured power-law exponents from all the runs. The exponents were calculated by fitting power-law solutions $E_k \sim A_k k^{-\beta_K}$ and $E_m \sim A_m k^{-\beta_M}$ in the range $2k_u < k < \frac{3}{4}k_\nu$, where k_ν corresponds to the peak of the enstrophy spectrum $k^2 E_k$. The range of fitting can be seen in fig.3 by the vertical dotted lines. The bottom panel shows the distribution of these exponents in the range $1 < \mu < 20$, excluding run A12 and the A1-A3 dynamo runs. Although the dispersion of these values is quite large the exponents do not show much dependence on amplitude of

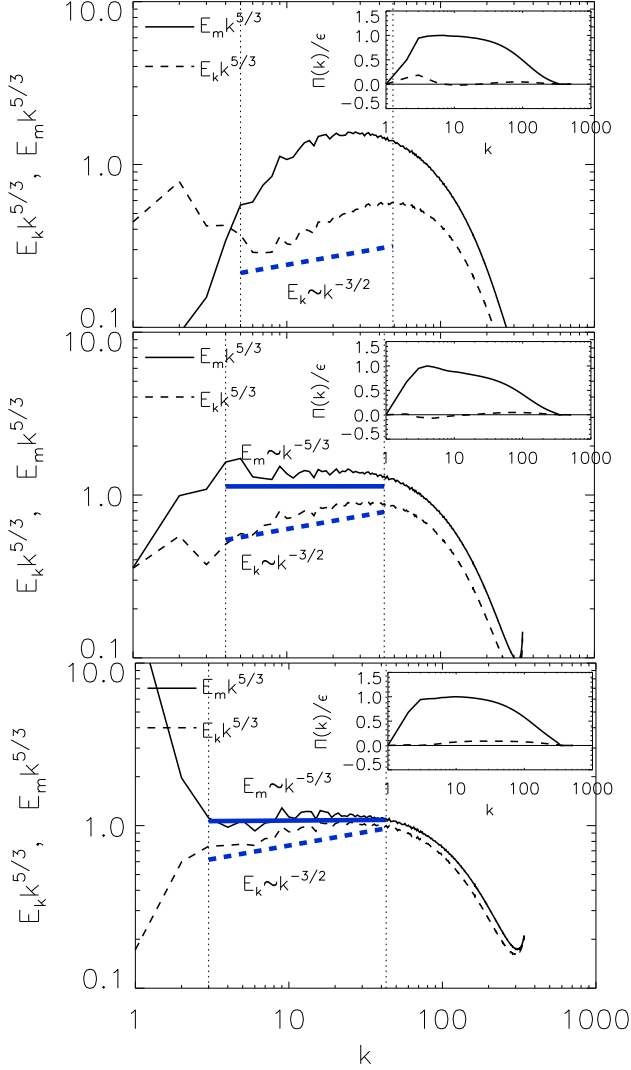


FIG. 3. Kinetic and magnetic compensated energy spectra for the Runs B1,B2,B3 (from top to bottom). The straight lines indicates the scaling $k^{-5/3}$ (solid) and $k^{-3/2}$ (dashed). The inset shows the energy flux $\Pi(k)$ (solid line) and $\Pi_u(k)$ (dashed line).

the magnetic field. Their values are concentrated around $k^{-5/3}$ for the magnetic energy spectrum and $k^{-3/2}$ for the kinetic energy spectrum in agreement with the high resolution runs.

Concluding, this work has showed an independence of the normalized energy dissipation rate ($\epsilon \propto U_{rms}^3 k_u$) and

spectral exponents ($\beta_M \simeq 5/3$ and $\beta_K \simeq 3/2$) on the amplitude of the large scale magnetic field over a large range of μ and for a variety of forcing configurations. Nonetheless, deviations were observed for very strong magnetic fields $\mu > 20$ (for which ($\epsilon \propto B_{rms} U_{rms}^2 k_b$)) and for fully helical flows that formed magnetic helicity condensates in the large scales. Analysis of higher order moments [7] and scale interactions [23] might shed more light in the processes that control MHD turbulence.

Aknowledgements. This work was performed

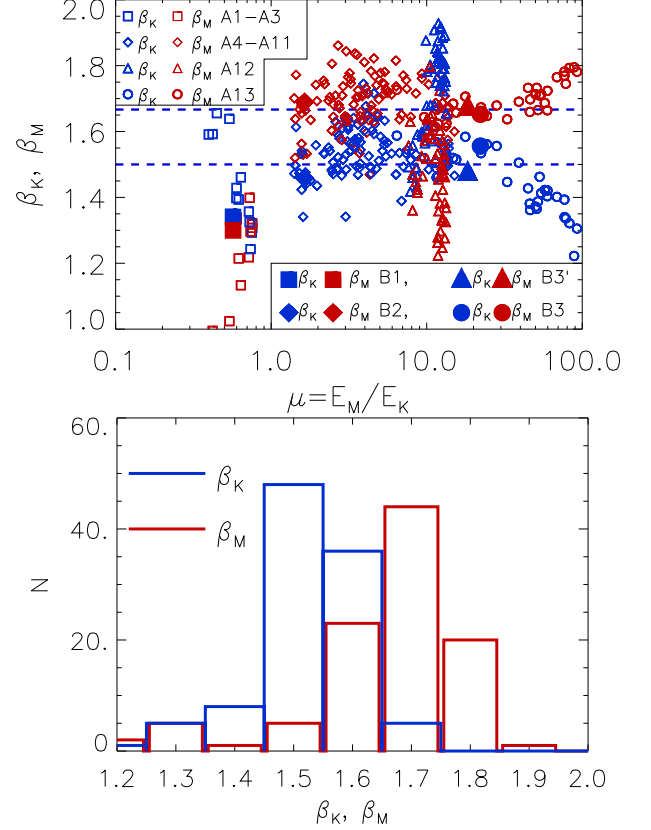


FIG. 4. Top panel: Measured exponents β_K and β_M for all runs. The exponents were calculated by a linear fit in the range $2k_u < k < \frac{3}{4}k_\nu$, where k_{nu} corresponds to the peak of the energy spectrum. Bottom panel: Distribution of the measured exponents for all runs in the range $1 < E_M/E_K < 20$, excluding run A12 and A1-A3.

using HPC resources from GENCI-CINES (Grant 2012026421).

[1] A. Kolmogorov, Dokl. Akad. Nauk SSSR **31**, 583 (1941)
 [2] S. Goto and J. C. Vassilicos, Phys. of Fluids **21**, 035104 (2009)
 [3] Y. Kaneda, T. Ishihara, M. Yokokawa, K. Itakura, and A. Uno, Phys. of Fluids **15**, L21 (2003)
 [4] K. R. Sreenivasan, Phys. of Fluids **7**, 2778 (1995)

[5] S. V. Nazarenko, *Wave Turbulence* (Springer-Verlag, 2011)
 [6] Y. Zhou, W. H. Matthaeus, and P. Dmitruk, Reviews of Modern Physics **76**, 1015 (2004)
 [7] D. Biskamp, *Magnetohydrodynamic Turbulence* (Cambridge University Press, 2003)

- [8] Y. B. Zeldovich, A. A. Ruzmaikin, and A. A. Sokoloff, *Magnetic Fields in Astrophysics* (Gordon and Breach, 1990)
- [9] P. A. Davidson, *An introduction to Magnetohydrodynamics* (Cambridge University Press, 2001)
- [10] S. Galtier, S. V. Nazarenko, A. C. Newell, and A. Pouquet, *J. Plasma Phys.* **13**, 447 (2000)
- [11] P. S. Iroshnikov, *Astron. Zh* **40**, 742 (1963)
- [12] R. H. Kraichnan, *Phys. Fluids* **8**, 1385 (1965)
- [13] A. Alexakis, B. Bigot, P. H., and S. Galtier, *Phys. Rev. E* **76**, 056313 (2007)
- [14] P. Goldreich and S. Sridhar, *Astrophys. J.* **438**, 763 (1995)
- [15] S. Boldyrev, *Phys. Rev. Lett.* **96**, 115002 (2006)
- [16] A. Beresnyak, *Phys. Rev. Lett.* **106**, 075001 (2011)
- [17] J. Mason, J. C. Perez, S. Boldyrev, and F. Cattaneo, *Phys. of Plasmas* **19**, 055902 (2012)
- [18] J. C. Perez and S. Boldyrev, *Astrophys. J.* **672**, L61 (2007)
- [19] B. Bigot and S. Galtier, *Phys. Rev. E* **83**, 026405 (2011)
- [20] A. Alexakis, *Phys. Rev. E* **84**, 056330 (2011)
- [21] D. O. Gomez, P. D. Mininni, and P. Dmitruk, *Adv. Space Res.* **35**, 899 (2005)
- [22] D. O. Gomez, P. D. Mininni, and P. Dmitruk, *Phys. Scr. T* **116**, 123 (2005)
- [23] A. Alexakis, P. Mininni, and A. Pouquet, *Phys. Rev. E* **72**, 046301 (2005)